A phase field model for dislocation climb under irradiation: Formalism and applications to pure bcc iron and ferritic alloys

Gabriel-Franck Bouobda Moladje, Ludovic Thuinet, Charlotte Becquart, A. Legris

A phase field model for dislocation climb under irradiation: formalism and applications to pure bcc iron and ferritic alloys

Gabriel Franck Bouobda Moladje[a], Ludovic Thuinet[a,b,*], Charlotte S. Becquart[a,b], Alexandre Legris[a,b]

[a] *Univ. Lille, CNRS, INRAE, Centrale Lille, UMR 8207 - UMET - Unité Matériaux et Transformations, F-59000 Lille, France*
[b] *Laboratoire commun EDF-CNRS Etude et Modélisation des Microstructures pour le Vieillissement des Matériaux (EM2VM), France*

Abstract

A phase-field model allowing to describe dislocation climb under irradiation is presented. Whereas previous phase-field models of the literature devoted to this phenomenon only take into account vacancies, our approach includes the effect of self interstitial atoms (SIAs) as required in the context of irradiated metals. Beyond the fact that it rigorously ensures the balance between the quantity of point defects, vacancies and SIAs, absorbed or emitted by the loop and the loop evolution, the present model has several originalities. First, it is capable to quantify the climb rate for systems far from equilibrium, which is commonly the case under irradiation. This required supplemental methodological developments since we clearly show that a mere generalization of existing phase-field models is not satisfactory to tackle this specificity. Secondly, it alleviates the often adopted assumption of perfect sink through the introduction of a kinetic parameter related to the dislocation jog density. A preliminary generic study of dislocations considered as nonperfect sinks leads to nonintuitive results, since the climb rate decreases when the dislocation jog density increases. Thirdly, the

*Corresponding author
Email address: ludovic.thuinet@univ-lille.fr (Ludovic Thuinet)

possibility to consider different types of interacting microstructural defects in the model allows to show the significant role of the point defect thermal equilibrium fractions on the climb rate in pure bcc iron under irradiation conditions. Finally, the climb model is coupled to the chemical diffusion equations in the same phase-field formalism. For this purpose, a multi-time step algorithm is proposed in order to couple phenomena with different characteristic time scales by several orders of magnitude, namely climb, point defect and chemical diffusion. It allows to study the interaction between the motion of the dislocation and the well-known phenomenon of radiation induced segregation in a Fe-Cr alloy. It is shown that the shape and size of the solute atmosphere can strongly depend on the dislocation motion under irradiation.

Keywords: Phase-field, Dislocation climb, Irradiation, Radiation induced segregation

---

1. Introduction

Dislocation climb is a mechanism which contributes to plastic deformation of materials. The climb process occurs by absorption or emission of point defects (PDs) at the dislocation cores. This process is enhanced at high temperature due to the high PD concentration, especially vacancies, and becomes an essential part of high temperature creep. The PD absorption/emission by the dislocation takes place at specific defects along the dislocation line called jogs. In the case of high jog density, the kinetic of attachment/detachment of PD at dislocation cores is instantaneous compared to the PD diffusion towards dislocation. The local equilibrium of PD around the dislocation core is maintained along the dislocation line [1] and dislocations act as perfect sinks/sources. The climb process is then limited by the PD diffusion. For low jog density, the assumption of local equilibrium of PD along the dislocation line is no longer verified since, before being captured, the defect should migrate along the line towards

defected regions. The climb process is then limited by the mechanism of PD absorption/emission. The role of the dislocation climb has been put in evidence in different contexts, for example by studying the temperature-dependent deformations of crystals by means of crystal plasticity models [2–6] or the behaviour of grain boundary dislocations and their impact on the plastic deformation of polycristalline materials [7, 8].

Atomistic methods such as molecular dynamics (MD) are not well adapted to the study of dislocation climb as the diffusion of vacancies takes too much time compared to the typical time of a MD simulation. The other issue with MD or atomistic methods is the cohesive model used. Very few works have been published on these topics [9] and none of them concerns the type of alloys studied in this paper. Dislocation climb and vacancy diffusion have been included in discrete dislocation dynamics (DDD) which remains a tool of choice to simulate plasticity at the scale of individual dislocations [10–16]. However, steady-state climb conditions are adopted in most of the DDD models. Dislocation dynamics can also be studied in phase field (PF) models by considering the sheared volume as an order parameter [17–26] but most of them only deal with dislocation glide. Only recently PF models were proposed for dislocation climb [27–29]. The PF approach is particularly suitable to study this phenomenon because the diffusion process and the elastic interactions are naturally incorporated in its formalism. Moreover, one advantage of the PF models proposed so far is the possibility to alleviate the often adopted assumption of perfect sink through the introduction of a kinetic parameter related to the dislocation jog density. This specifity was illustrated by the investigation of the PD sink strength of low-angle symmetrical tilt grain boundaries under irradiation [30]. However, in these PF studies, the dislocation climb is only due to the vacancy diffusion and high temperatures are considered. The role of self-interstitial atoms (SIAs) on climb

is neglected, since the atomic fraction of SIAs at high temperature, in materials under typical conditions, remains low compared to that of vacancies. However, under irradiation, vacancies and SIAs are created in higher quantities and both contribute to dislocation climb. Despite the numerous PF models dedicated so far to microstructure evolutions under irradiation conditions [31–35], none of them tackles properly this issue.

Many phenomena are known to occur under irradiation due to PD diffusion towards microstructural defects (sinks): dislocation loop growth or shrinkage [33, 36], irradiation creep [37], radiation induced segregation (RIS) [38–40], swelling [41], etc. In alloys, the fluxes of chemical species are coupled to the ones of PDs and PD fluxes towards the sinks lead to RIS which consists in a local redistribution of alloying elements near the sinks. Recently, RIS at planar sinks mimicking grain boundaries was investigated by an atomic-based phase-field method in Fe-Cr alloys [39], its predictions being in good agreement with direct Atomic Kinetic Monte Carlo simulations for an extended range of Cr compositions and temperatures. Later, RIS was studied near an interstitial dislocation loop in Fe-Cr alloys using a PF approach [40]. The results obtained showed that RIS prediction depends strongly on the elastic interactions between PDs and dislocations. In this latter study [40], dislocations were considered to be perfect sinks and immobile. This is a questionable assumption which is justified if kinetics related to the PD and atom diffusion is faster than the dislocation climb rate. It is the case for PDs in most cases, but not always verified for atoms.

All these previous studies reported in the literature show that there is a need to develop a PF dislocation climb model under irradiation taking into account vacancies but also SIAs in order to correctly predict all the related phenomena, such as RIS. In the present work, we then propose a new PF formalism

of dislocation climb taking into account vacancy and SIA diffusion and absorption/emission at the dislocation cores. Like in the previous models described in [27–30], it ensures the balance between the quantity of PDs absorbed and the dislocation loop evolution due to a relevant choice of the conserved and not conserved order parameters and it allows to consider dislocations possibly as nonperfect sinks. It must be emphazised that the proposed model is not a mere generalization of the previous models for dislocation climb. Indeed, under irradiation, PD concentrations may be far from the equilibrium ones, which may induce spurious numerical effects on the evolution of the fields. An original contribution of this paper is then to propose a way to overcome the deficiencies encountered under irradiation. Thereafter, the growth of an interstitial loop mimicked by a dislocation dipole is simulated in pure bcc iron in the presence of another neutral sink. Indeed, considering different microstructural defects interacting with each other can be easily done in the PF framework of the model. Finally, we extend the method to binary alloys to investigate the effect of dislocation climb on the RIS prediction. This required the development of a multi-time step algorithm capable to couple phenomena with different characteristic time scales, namely climb, PD and chemical diffusion. This constitutes another original feature of the model.

The present paper is organized as follows. In section 2 the PF methodology is described. The model validation is presented in section 3 as well as its limitations and therefore some adjustments to the model are proposed. In section 4 the model is applied to simulate the growth of an interstitial dislocation loop in pure bcc iron, and then to investigate the dislocation climb effect on RIS prediction near a dislocation loop in Fe-Cr alloys.

2. Phase field methodology

The model consists in one dislocation loop that evolves by absorption/emission of PDs. The system is assumed free of any applied stress. To describe the system evolution, we define successively the order parameters, the total free energy of the system and the evolution equations, as usually done in a PF approach. The order parameters and the total free energy of the system are defined for a binary A-B alloy. The evolution equations are written first for a pure crystal and thereafter are generalized to a binary alloy.

The necessary order parameters to describe the system evolution are the following:

i. The atomic fraction of vacancies X_{V} and SIAs X_{I} inside the matrix.

ii. The atomic fractions X_A and X_B of chemical species A and B.

iii. The fields η^l_{V} and η^l_{I} which are related respectively to the atomic fraction of vacancies and SIAs absorbed or emitted by the loop.

iv. The order parameter η^l: classically, in PF methods a dislocation loop is identified on the boundary between a platelet of thickness d, within which the plastic field $\eta^l = 1$ and the matrix within which $\eta^l = 0$. The dislocation loop grows or shrinks through the net absorption/emission of SIAs or vacancies according to its type (interstitial/vacancy). Then, we define the order parameter η^l as follows:

$$\eta^l = \frac{1}{\mathrm{X}^*} sg(l)(\eta^l_{\mathrm{I}} - \eta^l_{\mathrm{V}}) \tag{1}$$

$sg(l) = 1$ for interstitial loop and -1 for vacancy loop, $\mathrm{X}^* = d/b$ is the number of PDs required for a unitary climb process, b is the length of the Burgers vector.

The total free energy of the system F is given by the sum of three contributions, namely the chemical energy F_{ch}, the dislocation core energy F_{core} and the elastic energy F_{el}:

$$F = F_{\mathrm{ch}} + F_{\mathrm{core}} + F_{\mathrm{el}} \tag{2}$$

The chemical free energy is given by:

$$F_{\mathrm{ch}}(X_\alpha, X_d) = \frac{\mathrm{k_B}T}{V_{\mathrm{at}}}\Big[\sum_\alpha \int_V X_\alpha \ln(\gamma_\alpha X_\alpha) dV + \sum_d \int_V X_d \ln(\frac{X_d}{X_d^{\mathrm{eq}}}) dV\Big] \tag{3}$$

where α stands for chemical species A and B, γ_α is the activity coefficient of alloying element α, V_{at} the atomic volume, $\mathrm{k_B}$ the Boltzmann constant, T the temperature of the system, and X_d^{eq} the PD atomic fraction at the thermal equilibrium, d stands for vacancies or interstitials. The dislocation core energy is expressed as the sum of a crystalline and a gradient energy term. A simple double-well function is used for the crystalline energy [27–29]. We suppose that the atomic fractions of A and B near the dislocation do not modify its core energy. Then, F_{core} only depends on η^l and is given by:

$$F_{\mathrm{core}}(\eta^l) = F_{\mathrm{cry}} + F_{\mathrm{grad}} = \int_V \Big[H(\eta^l)^2(1-\eta^l)^2 + \frac{\gamma}{2}|\boldsymbol{n} \wedge \boldsymbol{\nabla}\eta^l|^2\Big] dV \tag{4}$$

with $\boldsymbol{n}$ the normal to the habit plane of the loop. The coefficients H and γ control the dislocation core energy E_{core} and width w through the following expressions:

$$w = \sqrt{\frac{8\gamma}{H}}, \quad E_{\mathrm{core}} = b\sqrt{\frac{H\gamma}{12}} \tag{5}$$

The gradient of η^l is projected on the habit plane of the loop to eliminate any energy contribution along $\boldsymbol{n}$. The elastic energy is calculated via the microelasticity theory [42] and is a function of the elastic strain which is the difference

between the total strain $\varepsilon_{ij}(\boldsymbol{r})$ and the total eigenstrain $\varepsilon_{ij}^{0,\mathrm{tot}}(\boldsymbol{r})$:

$$F_{\mathrm{el}} = \frac{1}{2}\int_V C_{ijkl}[\varepsilon_{ij}(\boldsymbol{r}) - \varepsilon_{ij}^{0,\mathrm{tot}}(\boldsymbol{r})][\varepsilon_{kl}(\mathbf{r}) - \varepsilon_{kl}^{0,\mathrm{tot}}(\boldsymbol{r})] \quad dV \tag{6}$$

where C_{ijkl} are the elastic constants of the system which is assumed to be elastically homogeneous. The total eigenstrain $\varepsilon_{ij}^{0,\mathrm{tot}}$ is given by:

$$\varepsilon_{ij}^{0,\mathrm{tot}}(\boldsymbol{r}) = \sum_{\alpha} \varepsilon_{ij}^{0,X_\alpha} X_\alpha(\boldsymbol{r}) + \sum_{d} \varepsilon_{ij}^{0,X_d} X_d(\boldsymbol{r}) + \varepsilon_{ij}^{0,\eta^l} f(\eta^l(\boldsymbol{r})) \tag{7}$$

where ε_{ij}^{0,X_d}, $\varepsilon_{ij}^{0,X_\alpha}$ and $\varepsilon_{ij}^{0,\eta^l}$ are respectively the tensor of the Vegard's coefficients of PDs and of alloying elements, and the eigenstrain tensor of the loop. The PD relaxation volume Ω_d is related to ε_{ij}^{0,X_d} as follows:

$$\Omega_d = V_{\mathrm{at}}\,\mathrm{Tr}(\varepsilon_{ij}^{0,X_d}), \quad \text{with} \quad \mathrm{Tr}(\varepsilon_{ij}^{0,X_d}) = \sum_{i,j(i=j)} \varepsilon_{ij}^{0,X_d} \tag{8}$$

Nabarro [43] showed that a dislocation loop is elastically equivalent to a platelet inclusion with thickness d and whose border corresponds to the dislocation line, if the eigenstrain associated to the platelet $\varepsilon_{ij}^{0,\eta^l}$ is defined as:

$$\varepsilon_{ij}^{0,\eta^l} = \frac{b_i n_j + b_j n_i}{2d} \tag{9}$$

b_i and n_j are respectively the i^{th} component of the Burgers vector and the j^{th} component of the unit vector normal to the habit plane of the loop. $f(\eta^l)$ is an interpolation function defined as $f(\eta^l) = \eta^l$ and $f^{'}(\eta^l) = 0$ if η^l is an integer i.e. in the bulk and inside the loop. The derivative of $f(\eta^l)$ must be zero in the bulk and inside the loop to ensure that the elastic contribution does not modify the energy minima in these regions [28, 29]. A non-linear function which verifies

the properties listed above is given by [44, 45]:

$$f(\eta^l) = \eta^l - \frac{1}{2\pi}\sin(2\pi\eta^l) \tag{10}$$

The total strain $\varepsilon_{ij}(\boldsymbol{r})$ can be decomposed into two parts, the heterogeneous part of the strain $\delta\varepsilon_{ij}(\boldsymbol{r})$ and the average strain $\overline{\varepsilon}_{ij}$:

$$\varepsilon_{ij}(\boldsymbol{r}) = \overline{\varepsilon}_{ij} + \delta\varepsilon_{ij}(\boldsymbol{r}) \tag{11}$$

It can be demonstrated that in an elastically homogeneous system:

$$\overline{\varepsilon}_{ij} = \sum_{\alpha} \varepsilon_{ij}^{0,X_\alpha} \overline{X_\alpha(\boldsymbol{r})} + \sum_{d} \varepsilon_{ij}^{0,X_d} \overline{X_d(\boldsymbol{r})} + \varepsilon_{ij}^{0,\eta^l} \overline{f(\eta^l(\boldsymbol{r}))} \tag{12}$$

where $\overline{X_\alpha(\boldsymbol{r})}$, $\overline{X_d(\boldsymbol{r})}$ and $\overline{f(\eta^l(\mathbf{r}))}$ are respectively the volume average values of $X_\alpha(\boldsymbol{r})$, $X_d(\boldsymbol{r})$ and $f(\eta^l(\boldsymbol{r}))$. The heterogeneous strain $\delta\varepsilon_{ij}(\boldsymbol{r})$ is obtained by solving the mechanical equilibrium equation expressed in terms of the displacement field u_k:

$$C_{ijkl}\frac{\partial^2 u_k(\boldsymbol{r})}{\partial r_j \partial r_l} = C_{ijkl}[\sum_{\alpha} \varepsilon_{kl}^{0,X_\alpha} \frac{\partial X_\alpha}{\partial r_j}(\boldsymbol{r}) + \sum_{d} \varepsilon_{kl}^{0,X_d} \frac{\partial X_d}{\partial r_j}(\boldsymbol{r}) + \varepsilon_{kl}^{0,\eta^l} \frac{\partial f(\eta^l)}{\partial r_j}(\boldsymbol{r})] \tag{13}$$

where:

$$\delta\varepsilon_{ij}(\boldsymbol{r}) = \frac{1}{2}[\frac{\partial u_i}{\partial r_j} + \frac{\partial u_j}{\partial r_i}](\boldsymbol{r}) \tag{14}$$

Eq. 13 is solved in the Fourier space, as detailed in [18, 42, 46–48].

Considering a single crystal and as described in existing models [28, 29], during the exchange of PD between the loop and the matrix, the fields X_d and η_d^l are not conserved in the loop core neighborhood, but the system evolves such
115 that the total PD atomic fraction in the matrix and absorbed/emitted by the loop $\phi_d = X_d + \eta_d^l$ is conserved. The field ϕ_d is then a conserved parameter and

is governed by a Cahn-Hilliard-type equation. Moreover, η_d^l is a non-conserved order parameter and follows the Allen-Cahn equation usually used in PF models to simulate dislocation dynamics. The evolution equations are written according to the driving forces deriving from the total energy $F(X_\alpha, \phi_{\mathrm{I}}, \phi_{\mathrm{V}}, \eta_{\mathrm{I}}^l, \eta_{\mathrm{V}}^l)$:

$$\frac{\partial \phi_{\mathrm{I}}}{\partial t} = \boldsymbol{\nabla}.[M^{\mathrm{I}} \boldsymbol{\nabla} \frac{\delta F(X_\alpha, \phi_{\mathrm{I}}, \phi_{\mathrm{V}}, \eta_{\mathrm{I}}^l, \eta_{\mathrm{V}}^l)}{\delta \phi_{\mathrm{I}}}] \tag{15}$$

$$\frac{\partial \phi_{\mathrm{V}}}{\partial t} = \boldsymbol{\nabla}.[M^{\mathrm{V}} \boldsymbol{\nabla} \frac{\delta F(X_\alpha, \phi_{\mathrm{I}}, \phi_{\mathrm{V}}, \eta_{\mathrm{I}}^l, \eta_{\mathrm{V}}^l)}{\delta \phi_{\mathrm{V}}}] \tag{16}$$

$$\frac{\partial \eta_{\mathrm{I}}}{\partial t} = -L_{\eta^l}^{\mathrm{I}} \frac{\delta F(X_\alpha, \phi_{\mathrm{I}}, \phi_{\mathrm{V}}, \eta_{\mathrm{I}}^l, \eta_{\mathrm{V}}^l)}{\delta \eta_{\mathrm{I}}} \tag{17}$$

$$\frac{\partial \eta_{\mathrm{V}}}{\partial t} = -L_{\eta^l}^{\mathrm{V}} \frac{\delta F(X_\alpha, \phi_{\mathrm{I}}, \phi_{\mathrm{V}}, \eta_{\mathrm{I}}^l, \eta_{\mathrm{V}}^l)}{\delta \eta_{\mathrm{V}}} \tag{18}$$

where M^d is the mobility of the PD defined as:

$$M^d = \frac{D^d X_d}{\mathrm{k_B} T} \tag{19}$$

$L_{\eta^l}^d$ denotes the coefficient that accounts for the kinetics of PD absorption/emission by the dislocation cores and can be chosen to reproduce quantitatively the climb rate of a jogged dislocation [29]. In our simulations, $L_{\eta^l}^d$ is assumed proportional to M^d in order to insure numerical stability:

$$L_{\eta^l}^d = \zeta_{\eta^l}^d M^d \tag{20}$$

The link between the PF parameter $L_{\eta^l}^d$ and the jog inter-spacing d_j (dislocation atomic scale property) is established in Section 2 of the Supplementary Materials. To write the evolution equations in function of the natural physical

order parameters $(X_{\mathrm{I}}, X_{\mathrm{V}}, \eta^l_{\mathrm{I}}, \eta^l_{\mathrm{V}})$, it is necessary to make a variable change from $F(X_\alpha, \phi_{\mathrm{I}}, \phi_{\mathrm{V}}, \eta^l_{\mathrm{I}}, \eta^l_{\mathrm{V}})$ to $F(X_\alpha, X_{\mathrm{I}}, X_{\mathrm{V}}, \eta^l_{\mathrm{I}}, \eta^l_{\mathrm{V}})$. The calculations are detailed in Section 1 of the Supplementary Materials and allow to obtain the following contracted evolution equations:

$$\frac{\partial X_d}{\partial t} = \boldsymbol{\nabla}.[M^d \boldsymbol{\nabla} \mu^d] - \frac{\partial \eta^l_d}{\partial t} \tag{21}$$

$$\frac{\partial \eta^l_d}{\partial t} = -L^d_{\eta^l}[\frac{1}{\mathrm{X}^*} sg(l) sg(d) \mu^{\eta^l} - \mu^d] \tag{22}$$

where $sg(d) = 1$ for SIAs and -1 for vacancies. The driving forces μ^d and μ^{η^l} are defined in Section 1 of the Supplementary Materials. Under this form, the right-hand side of Eq. 21 includes two distinct terms: the first one describes PD diffusion in the matrix driven by the gradient of the PD chemical potential and is the one used in the classical Cahn-Hilliard equation. More interestingly, the second term can be considered as an absorption term at dislocation cores which behaves like a sink for PDs. The time evolution of this absorption term depends on antagonist driving forces and deserves a few comments. For a loop absorbing PD of the same type (for example, an interstitial loop absorbing interstitials) the first term of the right-hand side of Eq. 22 is opposite to the growth of the loop (negative contribution to $\frac{\partial \eta^l_d}{\partial t}$), which can be easily understood physically: in the case of an interstitial loop, when interstitials are absorbed, it grows with an increase of the core and elastic energies of the loop, which is a barrier for growth. On the contrary, for an interstitial loop absorbing vacancies, this contribution becomes positive since vacancies induce a shrinkage of the loop. Concerning the second term, as soon as a significant PD supersaturation exists, the driving force μ^d, which is usually called the osmotic force, is positive.

The irradiation conditions are reproduced by adding an effective source term

of PD K_0^d in the evolution equation of X_d. The PDs recombination is neglected. To simulate the presence of another sink noted s, we introduced in the PD diffusion equation an additional absorption term. The sink s is assumed to not evolve due to the absorption of PDs, and immobile. The absorption term is defined as follows:

$$J_{s,d}^{\text{abs}}(\boldsymbol{r},t) = \lambda_s(\mathbf{r})\lambda_{\text{eff}}(X_d(\boldsymbol{r},t) - X_d^s) \tag{23}$$

where $\lambda_s(\boldsymbol{r})$ is the shape function associated to the capture region of the sink s, equal to 0 inside the matrix and 1 in the capture region. λ_{eff} is an efficiency factor equal to $1/\delta t$ in the case of a perfect sink, δt being the time step used to solve the kinetic equation of PD and to maintain X_d to X_d^s inside the sink. X_d^s is fixed at a constant value usually taken as the thermal equilibrium fraction of the PD.

In a binary A-B alloy, the evolution equations of the atomic fractions of PDs and chemical species are given by [38–40]:

$$\frac{\partial X_d}{\partial t} = -V_{\text{at}}\boldsymbol{\nabla}.\boldsymbol{J}_d(\boldsymbol{r},t) \tag{24}$$

$$\frac{\partial X_\alpha}{\partial t} = -V_{\text{at}}\boldsymbol{\nabla}.\boldsymbol{J}_\alpha(\boldsymbol{r},t) \tag{25}$$

where $\boldsymbol{J}_d$ and $\boldsymbol{J}_\alpha$ are respectively the fluxes of PDs and chemical species. These fluxes are related to the fluxes $\boldsymbol{J}_\alpha^d$ of chemical species α mediated by PDs d through the following equations:

$$\boldsymbol{J}_d = sg(d)\sum_\alpha \boldsymbol{J}_\alpha^d, \quad \boldsymbol{J}_\alpha = \sum_d \boldsymbol{J}_\alpha^d \tag{26}$$

In the framework of the thermodynamics of irreversible processes (TIP) [49],

$\boldsymbol{J}_{\alpha}^{d}$ are assumed to be a linear combination of the thermodynamic driving forces $\boldsymbol{\nabla}\mu^{\beta}$ and $\boldsymbol{\nabla}\mu^{d}$, and the Onsager kinetic coefficients $L_{\alpha\beta}^{d}$:

$$\boldsymbol{J}_{\alpha}^{d} = -\sum_{\beta} L_{\alpha\beta}^{d}(\boldsymbol{\nabla}\mu^{\beta} + sg(d)\boldsymbol{\nabla}\mu^{d}) \tag{27}$$

The Onsager matrix of coefficients $L_{\alpha\beta}^{d}$ is symmetric and positive [50], and depends on temperature, alloy composition, and internal/external stresses. The evolution equations become, by taking into account the effective PD generation rates, the dislocation climb and the presence of another sink s:

$$\frac{\partial X_d}{\partial t} = \boldsymbol{\nabla}.[\sum_{\alpha}\sum_{\beta} \frac{l_{\alpha\beta}^{d} X_d}{\mathrm{k_B}T}(sg(d)\boldsymbol{\nabla}\mu^{\beta} + \boldsymbol{\nabla}\mu^{d})] - \frac{\partial \eta_d^l}{\partial t} - J_{s,d}^{\mathrm{abs}} + K_0^d \tag{28}$$

$$\frac{\partial \eta_d^l}{\partial t} = -L_{\eta^l}^{d}[\frac{1}{\mathrm{X}^*} sg(l)sg(d)\mu^{\eta^l} - \mu^{d}] \tag{29}$$

$$\frac{\partial X_\alpha}{\partial t} = \boldsymbol{\nabla}.[\sum_{d}\sum_{\beta} \frac{l_{\alpha\beta}^{d} X_d}{\mathrm{k_B}T}(\boldsymbol{\nabla}\mu^{\beta} + sg(d)\boldsymbol{\nabla}\mu^{d})] \tag{30}$$

where $l_{\alpha\beta}^{d}$ are the coefficients of the normalised Onsager matrix given by:

$$l_{\alpha\beta}^{d} = \frac{V_{\mathrm{at}}\mathrm{k_B}T}{X_d} L_{\alpha\beta}^{d} \tag{31}$$

$J_{s,d}^{\mathrm{abs}}$ is given by Eq. 23.

The following dimensionless parameters are introduced to solve Eqs. 28 -

30:

$$\begin{cases} F^* = F/H, \quad \mu^* = \mu/V_{\mathrm{at}}H \\ l^{d,*}_{\alpha\beta} = l^d_{\alpha\beta}t_0/a_0^2, \quad \zeta^{d,*}_{\eta^l} = HV_{\mathrm{at}}a_0^2\zeta^d_{\eta^l}/\mathrm{k_B}T \\ \boldsymbol{\nabla}^* = a_0\boldsymbol{\nabla}, \quad \boldsymbol{r}^* = \boldsymbol{r}/a_0, \quad \gamma^* = \gamma/(Ha_0^2) \\ t^* = t/t_0 \\ K_0^{d,*} = K_0^d t_0, \quad J^{\mathrm{abs},*}_{s,d} = t_0 J^{\mathrm{abs}}_{s,d} \end{cases} \tag{32}$$

where a_0 is the length of a unit PF cell, t_0 is the reference time chosen such that $t_0 = min(t_0^d, t_0^\alpha, t_0^{\eta^l})$ where t_0^d, t_0^α and $t_0^{\eta^l}$ are respectively the characteristic time associated to the PD diffusion, atom diffusion and dislocation motion:

$$t_0^d = \frac{a_0^2}{\mathrm{max}_r(D^d)} \tag{33}$$

$$t_0^\alpha = \frac{a_0^2}{\mathrm{max}_r(D^\alpha)} \tag{34}$$

$$t_0^{\eta^l} = \frac{a_0}{v_{\eta^l}} \tag{35}$$

max_r refers to the spatial maximum. The diffusion coefficient of atom D^α is given by [38, 39]:

$$D^\alpha = \phi \sum_d (\frac{l^d_{\alpha\alpha}}{X_\alpha} - \frac{l^d_{\alpha\beta}}{X_\beta})X_d - \sum_d sg(d)(\frac{l^d_{\alpha\alpha} + l^d_{\alpha\beta}}{X_\alpha})X_d \frac{\partial \ln X_d^{\mathrm{eq}}}{\partial \ln X_\alpha} \tag{36}$$

with ϕ the thermodynamic factor:

$$\phi = 1 + \frac{\partial \ln \gamma_\alpha}{\partial \ln X_\alpha} \tag{37}$$

The PD diffusion coefficients D^d are given by:

$$D^d = \sum_{\alpha}\sum_{\beta} l^d_{\alpha\beta}, \quad D^{d,*} = \sum_{\alpha}\sum_{\beta} l^{d,*}_{\alpha\beta} \tag{38}$$

v_{η^l} is the climb velocity which is estimated under irradiation conditions in Section 3 of the Supplementary Materials. In practice, t_0 corresponds to $a_0^2/max_r(D^{\mathrm{I}})$ due to the fact that SIA diffusion is generally faster than vacancy diffusion, atom diffusion and dislocation motion. The dimensionless evolution equations are:

$$\frac{\partial X_d}{\partial t^*} = \frac{V_{\mathrm{at}} H}{\mathrm{k_B} T}\boldsymbol{\nabla}^*.[\sum_{\alpha}\sum_{\beta} l^{d,*}_{\alpha\beta} X_d \boldsymbol{\nabla}^*(sg(d)\mu^{\beta,*} + \mu^{d,*})] - \frac{\partial \eta^l_d}{\partial t^*} - J^{\mathrm{abs},*}_{s,d} + K_0^{d,*} \tag{39}$$

$$\frac{\partial \eta^l_d}{\partial t^*} = -\zeta^{d,*}_{\eta^l} D^{d,*} X_d [\frac{1}{\mathrm{X}^*} sg(l) sg(d) \mu^{\eta^l,*} - \mu^{d,*}] \tag{40}$$

$$\frac{\partial X_\alpha}{\partial t^*} = \frac{V_{\mathrm{at}} H}{\mathrm{k_B} T}\boldsymbol{\nabla}^*.[\sum_{d}\sum_{\beta} l^{d,*}_{\alpha\beta} X_d \boldsymbol{\nabla}^*(\mu^{\beta,*} + sg(d)\mu^{d,*})] \tag{41}$$

These equations are spatially discretized using the staggered grid described in [39]. Generally the climb process, PD and atom diffusion occur at different time scales, the PD diffusion being much faster than the other phenomena. A multi-time step algorithm based on the one given in [39] is therefore required (see Section 4 of the Supplementary Materials) and used to accelerate the convergence towards the steady state, which allows to observe the evolution of the loop and of the atomic fractions of chemical species in a reasonable computation time.

For a given 2D edge dislocation dipole, the average value of η^l can be seen as the dipole volume fraction in the system:

$$\overline{\eta^l}_{\mathrm{dipole}} = \frac{V_{\mathrm{dipole}}}{V} \tag{42}$$

where V_{dipole} and V are respectively the representative volume of the dipole and the system volume. V_{dipole} is given by:

$$V_{\text{dipole}} = 2Ra_0^2 \tag{43}$$

with R the half of the distance between the dislocations. We have then:

$$\frac{\partial \overline{\eta^l}}{\partial t} = \frac{2a_0^2}{V}\frac{\partial R}{\partial t} \tag{44}$$

The climb rate is given by:

$$v_{\eta^l} = \frac{\partial R}{\partial t} = \frac{V}{2a_0^2}\frac{\partial \overline{\eta^l}}{\partial t} = \frac{Vsg(l)}{2a_0^2 \mathrm{X}^*}\left(\frac{\partial \overline{\eta_{\mathrm{I}}^l}}{\partial t} - \frac{\partial \overline{\eta_{\mathrm{V}}^l}}{\partial t}\right) = sg(l)(v_{\eta^l}^{\mathrm{I}} - v_{\eta^l}^{\mathrm{V}}) \tag{45}$$

with $v_{\eta^l}^d = \frac{V}{2a_0^2 \mathrm{X}^*}\frac{\partial \overline{\eta_d^l}}{\partial t}$. This last quantity is the contribution of PD d to the climb rate and will be used in the following to interpret the results.

3. PF model validation and limitations

The model is tested before its application to a real system to verify its validity and limitations. For this purpose, we model the growth of a prismatic interstitial loop by a net absorption of SIAs in a single crystal. For simplicity, subscript l has been suppressed in the notation of η. The loop is represented in 2 dimensions by a dipole of edge dislocations as illustrated in Fig. 1. The necessary parameters for the simulations are given in table 1. The initial profile of the order parameter η is schematized in Fig. 1-b).

The equilibrium atomic fraction of PD is set close to zero ($\mathrm{X}_d^{\text{eq}} = 10^{-30}$). The grid spacing a_0 and the platelet thickness d are taken equal to the length of the Burgers vector b. Two types of simulations are used to validate the model:

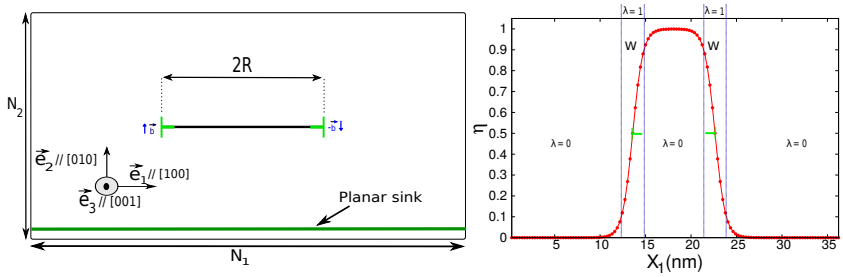

(a) (b)

Figure 1: a) 2D simulation domain of an interstitial dislocation loop and b) initial profile of η along the dipole.

T	700 K
b, a_0	0.3 nm
dislocation core energy	[1:10] eV.Å^{-1}
dislocation core width	2.4 nm
domain size	38.4 × 19.2 nm^2 (64 × 128 cells)
initial loop radius R_0	4.8 nm
Shear modulus μ	33 GPa
Poisson ratio ν	0.33
Atomic volume V_{at}	2.3×10^{-29} m^3
D_{I}, D_{V}	10^{-15} m^2.s^{-1}

Table 1: Parameters used for the PF climb model validation.

i. Simulation type 1: the system is assumed to be free of any other sinks ($\overline{J^{\text{abs}}_{s,d}} = 0$) and the PD effective generation rates are chosen non equal $K_0^{\text{I}} \neq K_0^{\text{V}}$.

ii. Simulation type 2: PDs are created at the same generation rate K_0 in the presence of another neutral sink s, which generates absorption differences between vacancies and interstitials by the loop.

Indeed, it is possible in these two cases to analytically calculate the climb rate of the dislocations, as demonstrated in Section 3 of the Supplementary Materials.

3.1. Validation without elastic interactions

The simulations of type 1 are performed firstly using the parameters of table 1 with $\zeta_\eta^{d,*} = 1$. At this stage, no elastic interactions between PDs and the dislocation are taken into account, i.e. $\varepsilon_{ij}^{0,X_d} = 0$. The PD effective generation rates are $K_0^{\mathrm{I}} = 4.45 \times 10^{-4}$ s^{-1} and $K_0^{\mathrm{V}} = 3.45 \times 10^{-4}$ s^{-1} which corresponds to an analytical climb rate of $v_\eta = 1.23 \times 10^{-10}$ m.s^{-1} (see Eq. S-40 of Section 3 of the Supplementary Materials). The average atomic fractions of PDs are plotted in Fig. 2-a) and do not reach any steady-state value, contrary to what is expected. The PD atomic fraction maps at t = 450 s show an unexpected

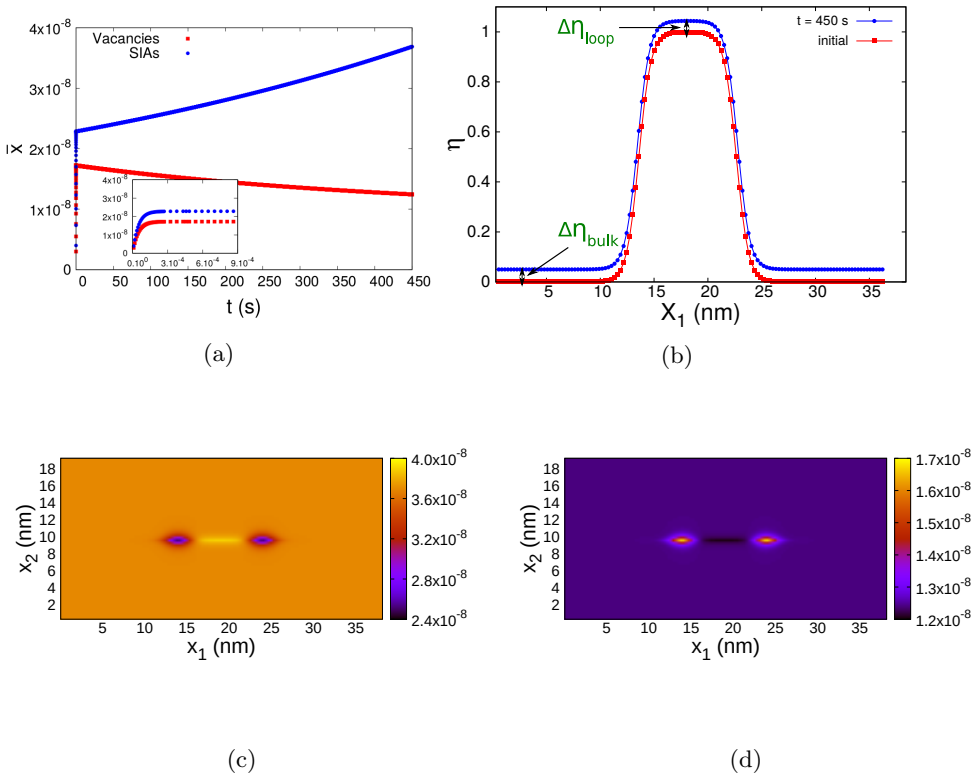

Figure 2: (Color online) a) Evolution of the average atomic fraction $\overline{\mathrm{X}}$ of PD. At t = 450 s, b) profile of η in the habit plane (x_2 = 9.6 nm), and atomic fraction maps of c) SIAs and d) vacancies in the case of simulation type 1 without elastic interactions.

behavior close to the dislocation cores. In particular, an enrichement is observed

at dislocation cores for vacancies (see Fig. 2-d). Moreover, there is a non physical enrichment (respectively depletion) of SIAs (respectively vacancies) in the habit plane of the loop. The field η at $t = 450$ s varies in the bulk and inside the loop as shown in Fig. 2-c) and adopts values different from 0 in the bulk and 1 inside the loop which explains the bad sink behavior. Examination of the evolution equation of η (see Eq. 22) shows that this particular profile of η is due to an unphysical osmotic force contribution far from the dislocation cores. Thus, the field η does not remain at its value 0 or 1 in the bulk and inside the loop. To overcome this spurious effect, we introduce a shape function $\lambda(\eta)$ as a factor of the osmotic force to ensure its value is zero outside the dislocation cores:

$$\lambda(\eta) = \begin{cases} 1 & \text{inside the core region} \\ 0 & \text{outside} \end{cases} \tag{46}$$

We made the choice to delimit the dislocation core region by $0.1 \leq \eta \leq 0.9$ as illustrated in Fig. 1-b). The evolution equation of 22 is rewritten as follows:

$$\frac{\partial \eta_d}{\partial t} = -L_\eta^d [\frac{1}{\mathrm{X}^*} sg(l) sg(d) \mu^\eta - \lambda(\eta) \mu^d] \tag{47}$$

The simulations are performed with this new formulation, keeping the same parameters as before. The atomic fraction maps of PD and the profile of η at steady state are plotted in Fig. 3. No shift from the values 0 and 1 in the bulk and inside the loop is observed on the profile of η and the atomic fraction maps show a qualitatively sound sink behavior of the dislocation cores. The average value of η is represented in Fig. 3 and its evolution is linear with time. The climb rate v_η is deduced from the slope of this curve and is equal to $1.33 \times 10^{-10} \mathrm{m.s}^{-1}$. This value is in good agreement with the one predicted analytically and allows to validate our model.

The influence of the coefficient ζ_η^d, which accounts for the kinetics of PD

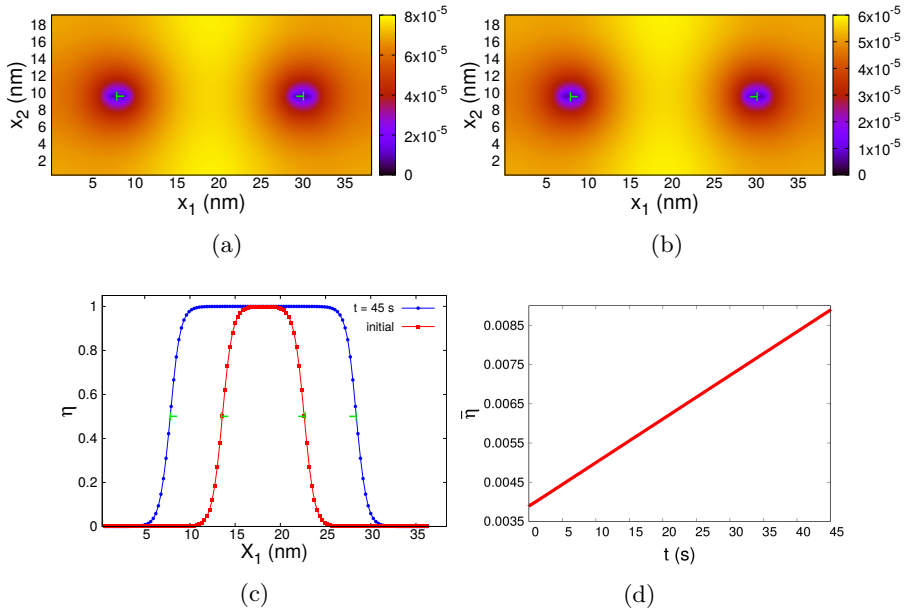

Figure 3: (Color online) Atomic fraction maps of a) SIAs, b) vacancies, and c) profile of η in the habit plane (x_2 = 9.6 nm) at t = 45 s, with the shape function $\lambda(\eta)$ as a factor of the osmotic force (simulation type 1 without elastic interactions). d) The corresponding evolution of $\overline{\eta}$ as a function of time.

absorption at the dislocation cores, is then investigated. The average atomic fraction of PD is plotted in Fig. 4 as a function of time for differents values of $\zeta_\eta^{d,*}$. This figure shows a decrease of the average atomic fraction when $\zeta_\eta^{d,*}$ increases. Oscillations are also observed and are probably due to the sharp shape of function $\lambda(\eta)$. This point is discussed in section 5. The profiles of the PD atomic fraction along the dipole given in Fig. 4-c) and d) show that X_d stays close to the equilibrium value ($X_d^{\text{eq}} \simeq 0$) in the vicinity of the dislocation cores when $\zeta_\eta^{d,*}$ is high, which is consistent with the fact that, for a high jog density, the local equilibrium of PD around the dislocation cores is maintained [1] and dislocation cores act as perfect sinks.

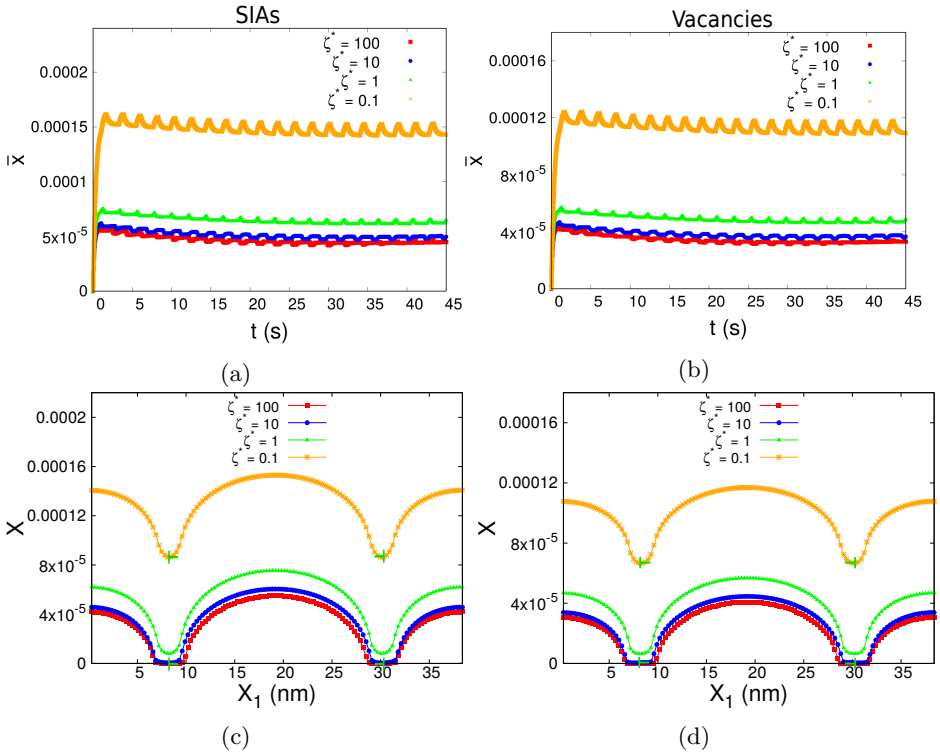

Figure 4: (Color online) Average atomic fraction of a) SIAs and b) vacancies as a function of time and atomic fraction profile in the habit plane (x_2 = 9.6 nm) of c) SIAs and d) vacancies at t = 45 s, without elastic interactions for differents values of $\zeta_\eta^{d,*}$ in the case of simulation type 1.

3.2. Validation with elastic interactions

The simulations of type 1 are performed taking into account the elastic interactions with $\zeta_\eta^{d,*} = 100$ (perfect sink) and the same PD generation rates as in section 3.1. The tensor of the vegard's coefficients of PDs is taken isotropic and the corresponding relaxation volumes are $\Omega_{\mathrm{I}} = 1.2\mathrm{V}_{\mathrm{at}}$ and $\Omega_{\mathrm{V}} = -0.6\mathrm{V}_{\mathrm{at}}$, which correspond to elastic parameters of a model material necessary for validation tests. The time evolution of $\overline{X}_d$ is plotted in Fig. 5, together with the maps of X_d and the profile of η along the dipole at $t = 31.5$ s. The PD atomic fraction map of SIAs shows an enrichment in the tension region of the dislocations and depletion in the compression region which is expected, while the opposite be-

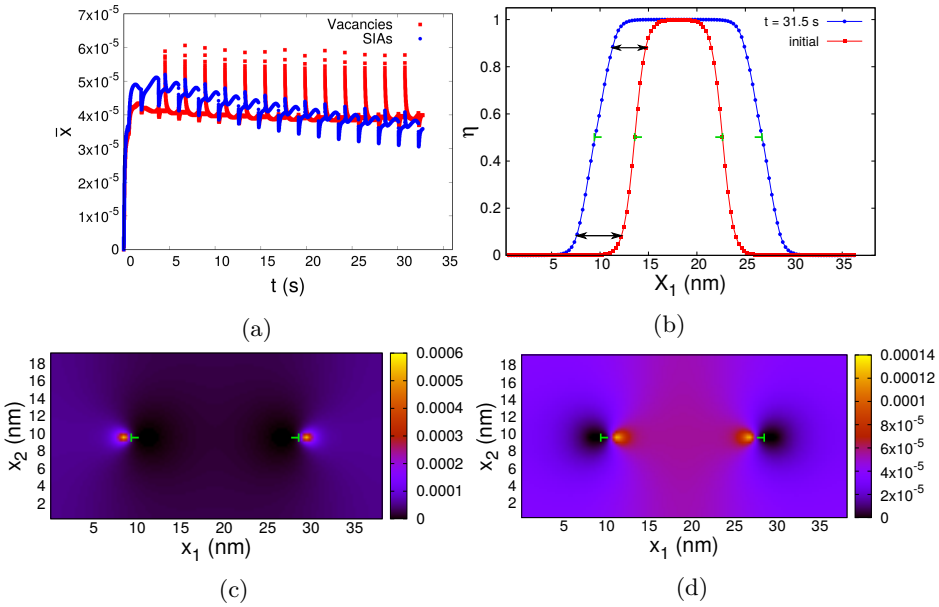

Figure 5: (Color online) a) Evolution of the average atomic fraction $\overline{\mathrm{X}}$ of PD. At t = 31.5 s, b) profile of η along the dipole ($x_2 = 9.6$ nm), and atomic fraction maps of c) SIAs, d) vacancies with elastic interactions in the case of simulation type 1.

havior is observed in the case of vacancies: the overall absorption of SIAs by an interstitial loop leads to the loop growth while the vacancies absorption leads to the loop shrinkage. As the local distribution of X_d around the dislocation cores is heterogeneous due to elasticity, the evolution of η is also heterogeneous along the interface as shown in Fig. 5-c) due to the dependence of L_η^d with X_d (see Eqs. 19 and 20). The part of the interface located in the tension zone moves faster than the other one located in the compression zone. This induces strong oscillations of $\overline{X}_d$ as shown in Fig. 5-a). To conserve the shape of η during the loop evolution and suppress these spurious oscillations, the average value of X_d is considered inside the core region to compute L_η^d (see Eq. 20) during the temporal integration of the evolution equation of η_d:

$$\eta_d(t+\delta t) = \eta_d(t) + [\frac{\partial \eta_d}{\partial t}]^{\mathrm{corr}} \delta t + \tau \tag{48}$$

where

$$[\frac{\partial \eta_d}{\partial t}]^{\text{corr}} = -\zeta_\eta^{d,*} D^{d,*} X_d^{\text{corr}} [\frac{1}{\mathrm{X}^*} sg(l) sg(d) \mu^{\eta,*} - \lambda \mu^{d,*}] \tag{49}$$

with

$$X_d^{\text{corr}} = \begin{cases} \frac{\int_V \lambda X_d dV}{\int_V \lambda dV} & \text{inside the core region} \\ \\ X_d & \text{outside} \end{cases} \tag{50}$$

τ is a corrective term that ensures the conservation of the field $X_d + \eta_d$:

$$\tau = (\lambda/\overline{\lambda})(\overline{[\frac{\partial \eta_d}{\partial t}]^{\text{corr}}} - \overline{\frac{\partial \eta_d}{\partial t}})\delta t \tag{51}$$

The dislocation core energy E_{core} can be also artificially increased to conserve the shape of η as suggested by Geslin [51]. The dislocation core structure which is modelled as a diffuse interface is modified due to the elastic interactions. Typically, the dislocation core energy is increased in our simulations by a factor within the range of values 1-10. The application of Eq. 48 to conserve the shape of η leads to $\overline{X}_d$, the maps of X_d and the profile of η along the dipole plotted in Fig. 6. Taking the effective dislocation core energy $E_{\text{core}}^{\text{eff}} = 8E_{\text{core}}$, the interface width w is conserved. The profile of η (see Fig. 6-b) shows its shape conservation during dislocation climb. The PD atomic fraction maps are also different from that of Fig. 5. In particular, the SIA (respectively vacancy) enrichment in the tension (respectively compression) zone is significantly attenuated.

To investigate the effects of ζ_η^d on the climb rate in presence of elastic interactions, simulations of type 2 were performed. PDs are created at the same effective generation rate $K_0 = 3.45 \times 10^{-4}\mathrm{s}^{-1}$. Due to the choice of Ω_{I} and Ω_{V} ($|\Omega_{\mathrm{I}}| > |\Omega_{\mathrm{V}}|$), edge dislocations should absorb more SIAs than vacancies in the presence of a neutral sink (see Section 3 of the Supplementary Materials). To investigate this situation, a neutral planar sink is introduced in the system

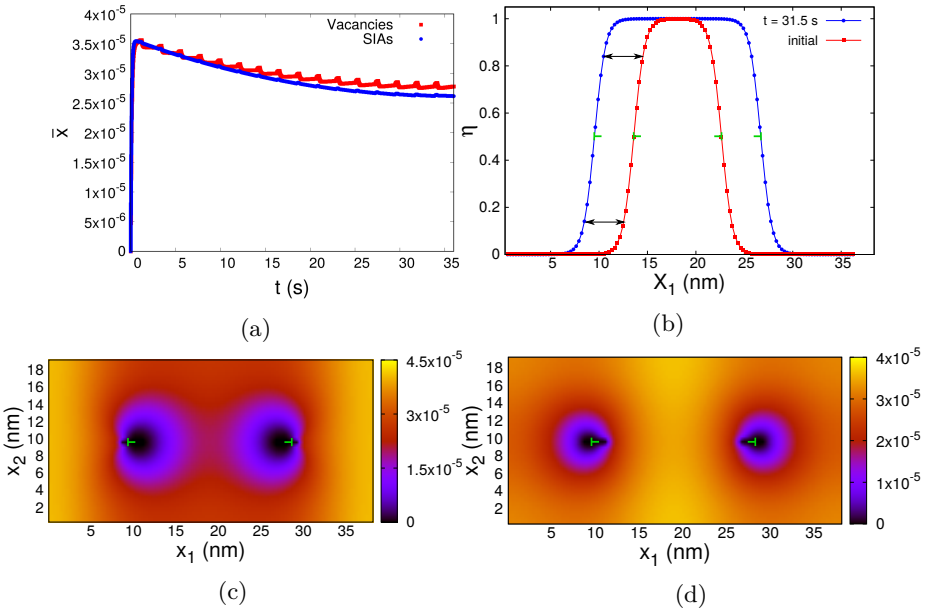

Figure 6: (Color online) a) Evolution of the average atomic fraction $\overline{\mathrm{X}}$ of PD. At t = 31.5 s, b) profile of η along the dipole (x_2 = 9.6 nm), and atomic fraction maps of c) SIAs and d) vacancies, with elastic interactions after application of Eq. 48 to conserve the shape of η (simulation type 1).

as illustrated on Fig 1. The simulations were performed for different values of $\zeta_\eta^{d,*}$ ($\zeta_\eta^{\mathrm{V},*} = \zeta_\eta^{\mathrm{I},*}$). Figs. 7-a) and 7-b) show a decrease of the average atomic fraction at the stationary state when $\zeta_\eta^{d,*}$ increases like in the case of simulation type 1 (see Fig. 4). The average value of η as well as the climb rate decreases when $\zeta_\eta^{d,*}$ increases as shown in Fig. 7. This can be explained as follows: when $\zeta_\eta^{d,*}$ increases, the kinetics of PD attachment at dislocation cores increases also. Thus, the absorption rate of PD at steady state increases with $\zeta_\eta^{d,*}$, which leads to the increase of the climb rate through vacancy and SIA absorption $v_{\eta^l}^{\mathrm{I}}$ and $v_{\eta^l}^{\mathrm{V}}$ as shown in Fig. 8. The increase of the climb rate with $\zeta_\eta^{d,*}$ via the vacancy absorption $v_{\eta^l}^{\mathrm{V}}$ is more important than via the SIA absorption $v_{\eta^l}^{\mathrm{I}}$, which is a non trivial result. In fact, as SIAs are more attracted towards the dislocation cores than vacancies due to the elastic drift term ($|\Omega_{\mathrm{I}}| > |\Omega_{\mathrm{V}}|$), the rate absorption of SIAs is therefore less affected by the variations of $\zeta_\eta^{d,*}$ than the rate absorption

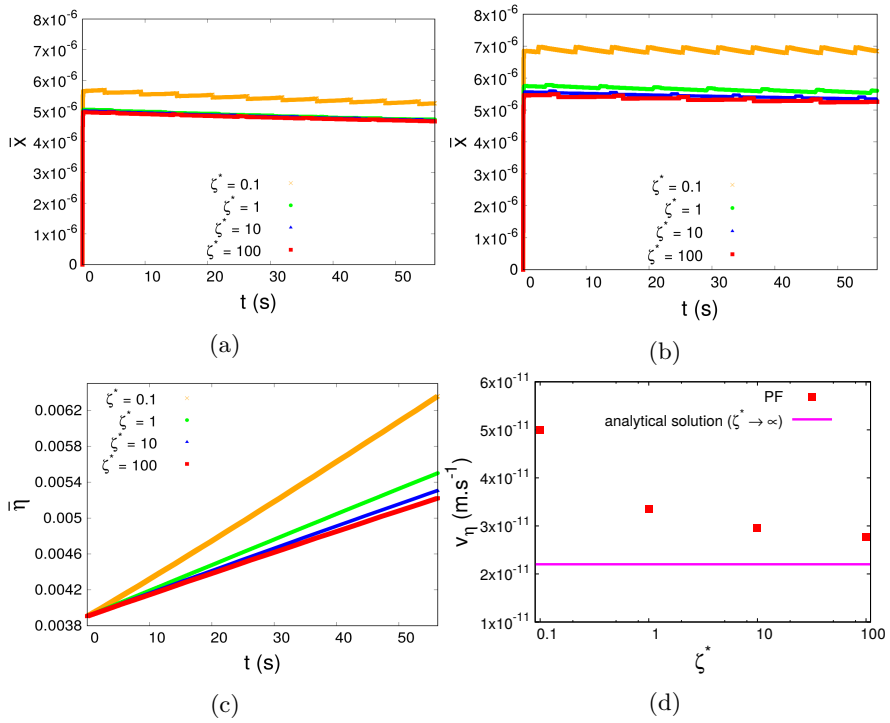

Figure 7: (Color online) Average atomic fractions of a) SIAs, b) vacancies, c) the average value of η and d) the climb rate as a function of ζ^* in the case of simulation type 2 (dipole of edge dislocations and planar sink).

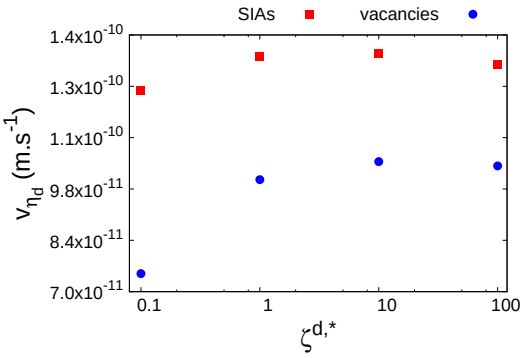

Figure 8: (Color online) Climb rate through the SIA and vacancy diffusion as a function of $\zeta^{d,*}$ in the case of simulation type 2 (dipole of edge dislocations and planar sink), $v_{\eta_d} = \frac{V}{2a_0^2}\frac{\partial \overline{\eta_d}}{\partial t}$ (see Eq. 44).

of vacancies, since the rate absorption depends also on the PD flow towards the sinks. Finally, the overall climb rate (i.e. the difference between the climb rate via SIA diffusion and vacancy diffusion) decreases when $\zeta_\eta^{d,*}$ increases. The analytical solution of the climb rate established in Section 3 of the Supplementary Materials for this type of simulation is also represented on Fig. 7-d) in the case of perfect sinks ($\zeta^* \to \infty$). This figure shows that the good order of magnitude of the climb rate is obtained in our simulations, but a discrepancy is observed between the PF results and the analytical solution, even for large values of ζ^*. This discrepancy may be due to the fact that the model of Rauh and Simon [52] is used to compute the dislocation sink strength in the analytical solution whereas this model is known to deviate from the PF solution, as already shown and explained in [34].

4. Applications

4.1. Growth of a prismatic interstitial loop in pure bcc Fe

Experimental studies [53–55] show that under neutron-irradiation, more interstitial loops are observed than vacancy loops in α-Fe. In particular <100>-type loops are often observed at high temperatures ($T > 573$ K). The growth of a <100>-type interstitial loop is thus simulated by performing simulation of type 2 as described in section 3 (see Fig. 1). The PD irradiation rate is $K_0 = 10^{-5}$ dpa.s^{-1}. The physical parameters of table 2 are used and ζ_d^* is fixed to 400 for both PDs to reproduce a perfect sink behavior by dislocation cores. The PD diffusion coefficient D^d and thermal equilibrium fraction X_d^{eq} are taken from [39].

Simulations are first performed for different temperatures. $\mathrm{X}_d^{\mathrm{eq}}$ are fixed to zero (typically 10^{-30}) and to their more realistic values calculated in [39] to investigate their effects on the climb rate. In Fig. 9 is represented the climb

b	2.83 Å
dislocation core energy	8 eV.Å^{-1}
dislocation core width	2.264 nm
domain size	36.2 × 18.1 nm^2 (64 × 128 cells)
initial loop radius R_0	4.528 nm
C_{11}, C_{12}, C_{44}	243, 145, 116 GPa [56, 57]
Ω_i, Ω_v	1.86V_{at}, -0.3V_{at}
V_{at}	1.13×10^{-29} m^3

Table 2: Physical parameters for applications.

rate as a function of the temperature. It can be seen that for $X_d^{eq} = 10^{-30}$ the climb rate decreases linearly with the temperature, in agreement with the analytical solution. For X_d^{eq} close to zero, the analytical solution given by Eq. S-46 of Section 3 of the Supplementary Materials depends only on the sink strength, V and K_0 being fixed. Thus, as the dislocation sink strength decreases with temperature due to the attenuation of the elastic effects, the climb rate decreases also. When the real PD thermal equilibrium fractions are considered, Fig. 9 shows a decrease followed by an increase of the climb rate with the temperature. This evolution of the climb rate with the temperature can be explained as follows: at low temperatures $T < 800$ K, the average fraction $\bar{X}_d$ at steady state is far from the thermal equilibrium fraction for both PDs as shown in Fig. 9-b) and c). There is thus an important osmotic driving force for climb for both PDs due to the large excess of PD fraction available in the bulk. The climb rate evolution with temperature is therefore mainly controlled by the elastic interactions in this range of temperature. Consequently, the climb rate decreases with the temperature for $T < 800$ K, like in the case of the previous simulations for which $X_d^{eq} = 10^{-30}$. For high temperatures $T > 800$ K, the vacancy fraction at steady state doesn't exceed anymore the thermal equilibrium value (see Fig. 9-b)), while the opposite behavior is observed for SIAs (see Fig. 9-c)), since the SIA thermal equilibrium fraction remains small. The osmotic

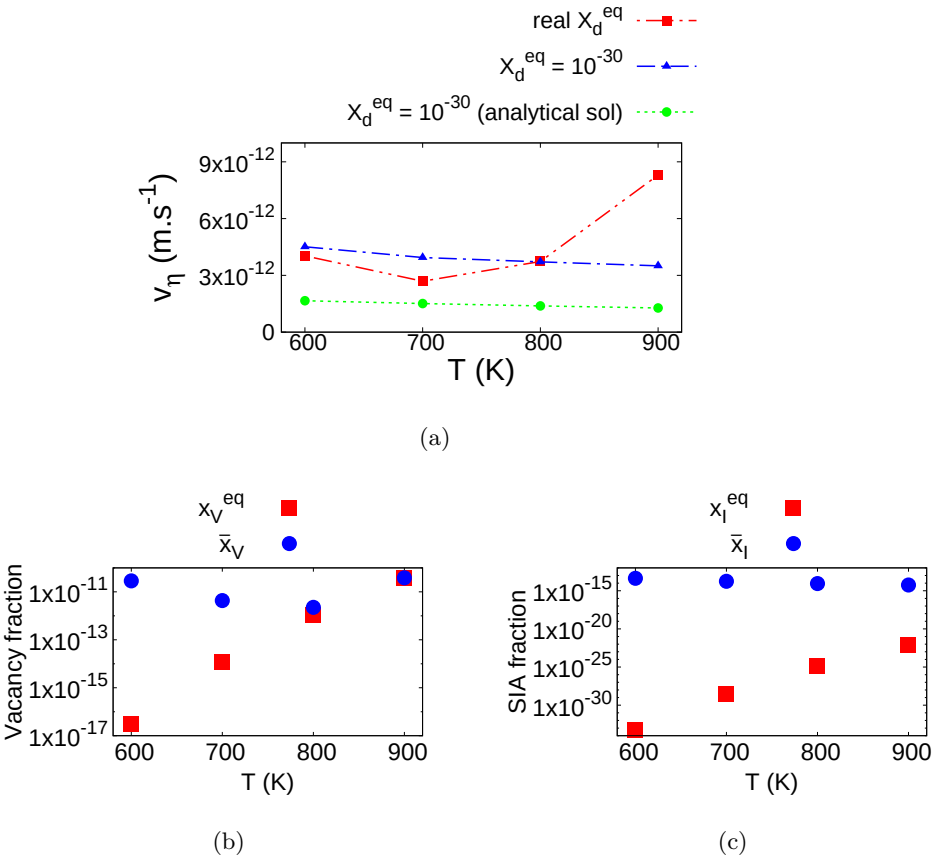

Figure 9: (Color online) a) Climb rate of a <100>-type interstitial loop as a function of the temperature in the case of simulation type 2, for a dislocation density of $3.048 \times 10^{15}\mathrm{m}^{-2}$ and an interplanar spacing of 18 nm. PD fraction as a function of the temperature at thermal equilibrium and at steady state in the PF simulations of type 2 for b) vacancies and c) SIAs.

force due to vacancy tends to zero in this range of temperature ($T > 800$ K), while the one due to SIAs remains significant. Since the osmotic force due to vacancy contributes to the decrease of the climb rate of the interstitial loop, its decrease with the temperature leads therefore to the climb rate increase. These results show that the PD equilibrium fraction plays a significant role on the loop growth rate estimation, especially at high temperatures.

The dislocation density effect on the climb rate is also investigated. The

evolution of the climb rate as a function of the dislocation density and the temperature is plotted in Fig. 10. This figure shows that the climb rate globally

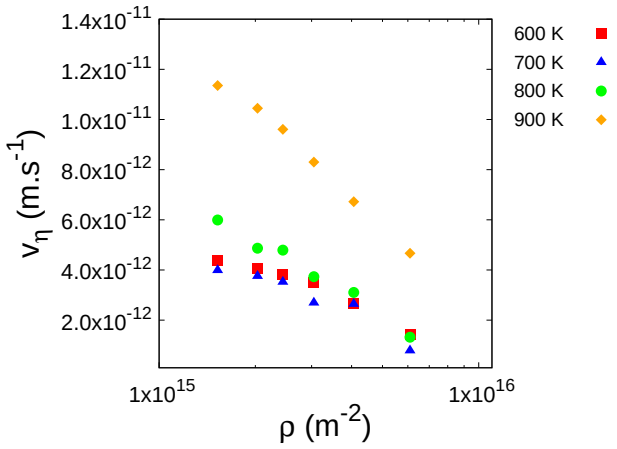

Figure 10: (Color online) Climb rate of a <100>-type interstitial loop as a function of the dislocation density and temperature, for an interplanar spacing of 18 nm (simulation type 2).

increases when the dislocation density decreases. Indeed, for small systems (high dislocation densities), the PD fraction in the bulk (reservoir) is weak at steady-state. The osmotic driving force for dislocation climb is then low which leads to low climb rates. Contrariwise, the greater the reservoir (low dislocation density), the more available PDs in the bulk. Thus, there is a high osmotic driving force and consequently a high climb rate.

4.2. RIS simulation near a prismatic interstitial loop in Fe-Cr alloys

Ferritic steels enriched in chromium are known to be good candidate materials for innovative nuclear reactor systems [58]. Indeed, these alloys have a good creep resistance. Furthermore, the high chromium content confers a good corrosion resistance. RIS is thus studied in this section near a <100> interstitial loop in Fe-11%Cr at 700 K by performing simulation of type 1 (i.e. the system is free of any other sinks and the PD generation rates are taken non equal) described

in section 2. The 2D simulation box of a <100>-type interstitial dislocation loop is illustrated in Fig. 1-a). The thermodynamic and kinetic parameters, namely the PD thermal equilibrium fraction X_d^{eq}, the Onsager coefficients $L_{\alpha\beta}^d$ and the thermodynamic factor ϕ, available in [39] are used. The other necessary parameters for the simulations are given in table 2. The PD relaxation volumes are taken from [59] ($\Omega_i = 1.1\mathrm{V_{at}}$, $\Omega_v = -0.05\mathrm{V_{at}}$). The eigenstrains of the chemical species are set to zero ($\epsilon_{ij}^{0,X_\alpha} = 0$) to ignore the elastic interactions produced by the small difference between the lattice parameters of iron and chromium. The dimensionless PF parameter $\zeta_{\eta^l}^{d,*}$ (see Eq. 20) is set to 100 for both PDs to reproduce a perfect sink behavior of dislocations. The following PD generation rates are chosen: $K_0^{\mathrm{I}} = 2 \times 10^{-5}\mathrm{dpa.s}^{-1}$ and $K_0^{\mathrm{V}} = 10^{-5}\mathrm{dpa.s}^{-1}$ which corresponds to a climb rate of $1.16 \times 10^{-11}\mathrm{m.s}^{-1}$. To investigate the climb rate effect on RIS prediction, simulations were performed in the static (temporal evolution equation of η^l is not integrated) and dynamic regimes of dislocations. In Fig. 11 are represented the atomic fraction maps of Cr in the static and dynamic regimes and the corresponding profiles along the dipole of dislocations at a dose of 0.012 dpa. In the static regime of dislocations, there is a Cr enrichment in the tension region of dislocations and Cr depletion in the compression region as shown in Fig. 11-a). This Cr segregation tendency can be explained by the following arguments [40]: vacancies are attracted in the compression zone of dislocations and expelled from the tension zone, while the opposite behavior is observed for SIAs. The fluxes of Cr atoms are coupled to the ones of PDs: in the same direction for SIAs and in the opposite direction for vacancies. As a consequence, Cr enrichment is due to SIAs and depletion due to vacancies. Thus, under elastic effects, Cr enrichment is expected in the tension region and Cr depletion in the compression region of dislocations. Without elasticity, Cr enrichment is obtained near dislocations [40] which means that Cr

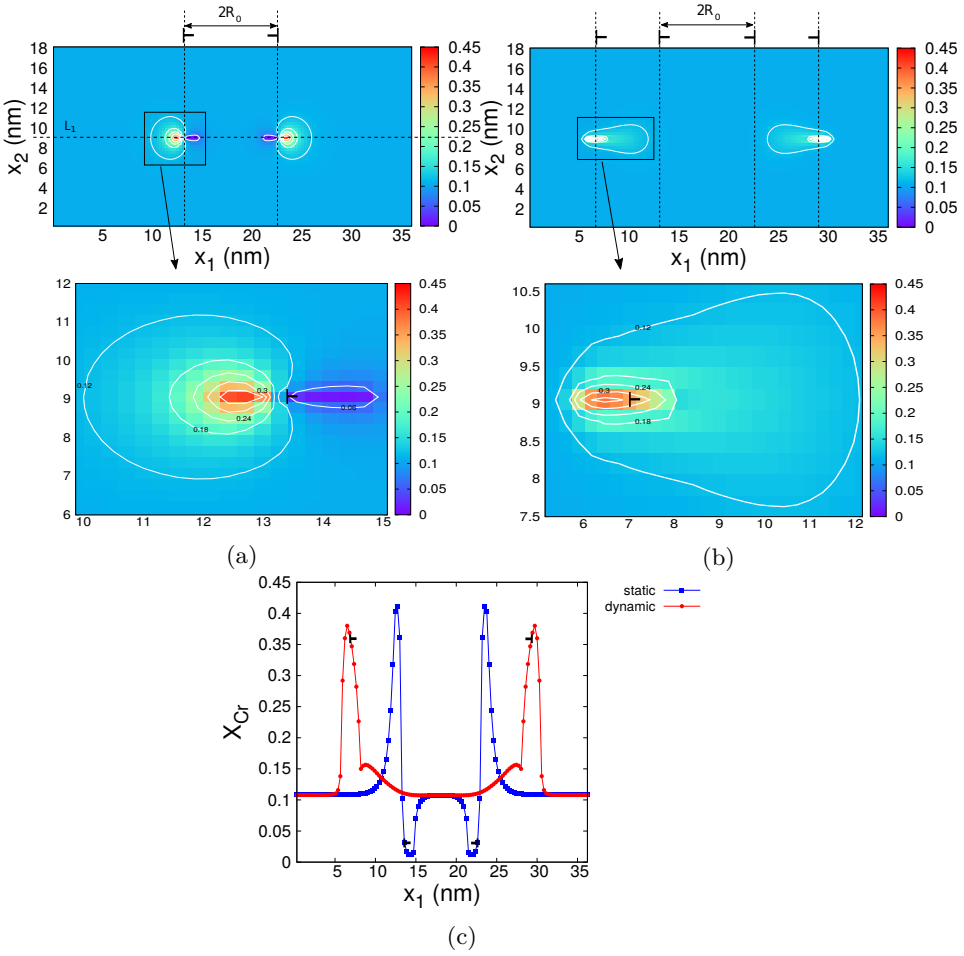

Figure 11: (Color online) Atomic fraction map of Cr for a) static and b) dynamic dislocations, and c) the corresponding profiles along L_1 axis at a dose of 0.012 dpa, in the kinetic regime where the atom diffusion is slower than the dislocation motion ($t_0^{\alpha} > t_0^{\eta}$) for Fe-11%Cr at 700 K, $K_0^{\mathrm{I}} = 2 \times 10^{-5}$ dpa.s^{-1} and $K_0^{\mathrm{V}} = 10^{-5}$ dpa.s^{-1}.

migrates preferentially through SIAs in Fe-11%Cr at 700 K. When elastic interactions are taken into account, both kinetic and elastic effects contribute to Cr enrichment in the tension zone. However, in the compression region, these both effects are antagonist and finally leads to Cr depletion. During the dynamic regime of dislocations, there is a significant change in the size and shape of the Cr atmosphere around dislocations as illustrated by the iso-concentrations rep-

resented on the Cr maps of Fig. 11. First, these iso-concentrations are flattened due to the motion of dislocations. The Cr segregation level is also affected by the dislocation motion as shown in Fig. 11-c), especially in the compression region where there is no more Cr depletion compared to the static profile for the dose reached. In order to understand this feature, the evolution of the Cr profile along the dipole as a function of the dose during the loop growth is plotted in Fig. 12. It can be seen that Cr profile similar to the static one (see

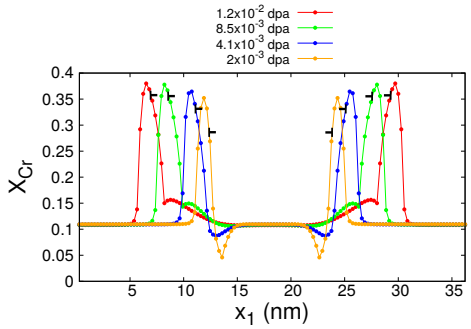

Figure 12: (Color online) Atomic fraction profile of Cr along L_1 axis for dynamic dislocations at different doses, in the kinetic regime where the atom diffusion is slower than the dislocation motion ($t_0^\alpha > t_0^\eta$) for Fe-11%Cr at 700 K, $K_0^{\mathrm{I}} = 2 \times 10^{-5}$ dpa.s^{-1} and $K_0^{\mathrm{V}} = 10^{-5}$ dpa.s^{-1}.

Fig. 11-c)) tends to be established at the beginning of the loop growth, with a Cr enrichment in the tension region and depletion in the compression region of dislocations. During the loop growth, Cr depletion in the compression region is no longer observed and there is only Cr enrichment in all sides of dislocations. This can be explained by the fact that the compression region moves towards the position where the tension region was previously during the loop growth. As the tension region was initially enriched in Cr, this region will become progressively depleted in Cr in order to establish the Cr segregation profile of the compression zone observed in the static case. However due to the faster motion of dislocations, the establishment of this Cr profile in the compression region (depletion) does not have time to fully occur (see Fig. 12).

To conclude, our results show that the climb rate can play an important

role on RIS prediction near dislocation cores. They also show that there is an interplay between the core mobility and the segregation profile.

5. Discussion

Several tests were carried out with our PF model of dislocation climb under irradiation. They showed that a mere generalization of existing models to SIAs and vacancies is not satisfactory in this case due to specificities related to irradiation conditions, in which the concentrations encountered may be far from the equilibrium ones. Some adjustments were therefore performed, like the introduction of a supplementary shape function $\lambda(\eta)$ given by Eq. 46 to ensure a nonzero osmotic force only at the dislocation cores. Before modifying the PF equations by using this shape function, preliminary tests not reproduced in this paper for brevity and clarity reasons have been performed in conditions close to equilibrium, i.e. with a point defect composition in the bulk close to the equilibrium ones (low supersaturations). Such conditions were reached by considering only vacancies at high temperatures, for which the equilibrium composition is much larger than those adopted in the simulation reproduced in Fig. 3. It turns out that in these specific conditions, η does not depart from 0 outside the loop and 1 inside the loop. These results obtained for low supersaturations are in accordance with those reported in [27, 28]. We then concluded that the problem comes from the osmotic force which reaches very large values in high supersaturation conditions, as the ones encountered under irradiation, even in zones where η is supposed to be 0 or 1. This hypothesis was confirmed by introducing the ad hoc function $\lambda(\eta)$ to suppress the osmotic force inside and outside the loop. It must be noticed that the shape function $\lambda(\eta)$ is an ad hoc function introduced in the model, and does not come from the variational derivation of the PF model described in section 2. A more physical approach could focus on

an alternative formulation of the free energy F allowing to introduce a counterpart of this shape function in the kinetic equations, but this is not a trivial question, especially in the general case corresponding to a chemical free energy given by Eq. 3.

As already mentioned in section 3.1, small oscillations are present on the time evolution of $\bar{X}_d$, the oscillations being due to the sharp shape of the function $\lambda(\eta)$. To suppress this numerical artifact, other smooth expressions of λ as a function of η have been tested but none of them were satisfactory. A more exhaustive investigation of this point is to be considered in future works, but since the relative amplitudes of these oscillations remain small, a step function for $\lambda(\eta)$ has been kept in all the simulations of this work.

The crystalline energy given by a double-well potential in Eq. 4 does not allow to simulate several loops (parameter η can not have integer values superior to 1). In order to include these configurations in the proposed formalism, one possibility is to replace the double-well potential by a periodic function of η for which a minimum of energy is reached for integer values of η. For simplicity reasons, we kept a double-well potential since Eqs. 5 are only valid in this case. These equations allow to control the core width and energy by means of the two input parameters H and γ in a simple and direct manner. In the case of more complex expressions of the crystalline energy, this calibration must be made numerically. Moreover, alternative expressions of function f used in Eq. 10 for the Burgers vector are also available in the literature and could be tested in the framework of this model. Indeed, Eq. 10 presents the shortcoming of requiring an infinite magnitude of stress to nucleate dislocation, which is not the case for the function of the Burgers vector proposed in [60].

Numerous parameters are introduced in the model, which is due to the fact that a lot of physical phenomena are included in the same formalism: diffusion of

the point defect and the chemical species with flux coupling, dislocation climb, elastic interactions. Most of them can be calculated by atomistic numerical methods or deduced from experiments but the L-coefficients introduced in Eqs. 17 and 18 and related to the mobility of the dislocation are undoubtedly the trickiest to determine. In section 2 of the Supplemental Materials, we establish the link between the L-coefficients and the following physical parameters: the jog interspacing on the dislocation d_j, the point defect diffusion coefficient in the bulk D_{B} and inside the dislocation D_{C}, and the exchange energy barriers from the bulk to the dislocation core $E_{\mathrm{B\text{-}C}}$ and from the dislocation core to the bulk $E_{\mathrm{C\text{-}B}}$. All these quantities related to the dislocations are difficult to determine. The jog interspacing on the dislocation could be estimated using MD simulations with very large boxes of different sizes so that the impact of the simulation box size (and the fact that periodic boundary conditions need to be used) could be assessed. As mentioned above, the results would depend on the quality of the cohesive model (the interatomic potential). Diffusion coefficients are difficult to estimate, especially in the dislocation core, and one would need to use off-lattice/self-learning Atomic Kinetic Monte-Carlo. All these technics are quite difficult to implement and the simulations take a long time. This is the reason why, in this paper, we did not try to determine precisely the L-coefficients, which is beyond the scope of this paper. Instead, we did a parametric study for values of ζ^* between 0.1 and 100, which corresponds to realistic values of these coefficients. For instance, adopting typical values for the related parameters ($E_{\mathrm{C\text{-}B}} = 0.4\mathrm{eV}$, $D^{\mathrm{v}}_{\mathrm{B}} = 1.13 \times 10^{-10}\mathrm{m}^2.\mathrm{s}^{-1}$, $D^{\mathrm{v}}_{\mathrm{C}} = 100 D^{\mathrm{v}}_{\mathrm{B}}$), a value of ζ^* equal to 0.1 corresponds to a jog interspacing of $60a$, a being the lattice parameter, for a climb rate of $1.2 \times 10^{-10}\mathrm{m.s}^{-1}$.

The model was applied to simulate first the growth of a <100>-type interstitial dislocation loop, represented in 2D by a dipole of edge dislocations, in

pure bcc iron. This growth was quantified by calculating the climb rate of dislocations. The effects of temperature and the dislocation density on the climb rate were investigated. The results showed a decrease of the climb rate followed by an increase when the temperature increases for a given dislocation density of $3 \times 10^{15} \mathrm{m}^{-2}$ and interplanar spacing of 18 nm (see Fig. 9). The evolution of the climb rate with the dislocation density showed overall an increase of the climb rate with the decrease of the dislocation density for all the temperatures (see Fig. 10). Our results under certain conditions are comparable to experimental observations.

The temperature dependence of the growth rate of interstitial loop in iron has been measured experimentally on a single thin foil by electron irradiation in [36]. The results show an increase of the growth rate as temperature increases and this increase was following an Arrhenius law as predicted by an analytical solution derived by the authors. Furthermore, a transmission electron microscopy (TEM) study of neutron irradiated iron [55] revealed a decrease of the dislocation density with the temperature increase. By taking into account this latter result, Fig. 10 shows that the climb rate increases with the combined effects of the increase of temperature and the decrease of the dislocation density, which is qualitatively in good agreement with the results obtained in [36]. Regarding the order of magnitude of the climb rate, by extrapolating the results of Fig. 10 to low dislocation densities, we can reach the range variation of $[10^{-11} - 10^{-9}]$ $\mathrm{m.s}^{-1}$ obtained in [36].

6. Conclusion

A new PF model of dislocation climb under irradiation, taking into account vacancies and SIAs diffusion and absorption/emission at the dislocation cores, has been developed and presented in this paper. On the methodological aspects,

this model presents several original features:

i. Whereas previous phase-field models of the literature devoted to dislocation climb only take into account vacancies, our approach includes the effect of self-interstitial atoms (SIAs) as required in the context of irradiated metals.

ii. It is capable to quantify the climb rate for systems far from equilibrium, which is commonly the case under irradiation. This required supplemental methodological developments since we clearly show in this paper that a mere generalization of existing phase-field models is not satisfactory to tackle this specificity. In particular, a shape function has been introduced to ensure the existence of the osmotic force only at the dislocation cores. The model has also been adjusted to overcome the modification of the dislocation core structure due to elasticity.

iii. It alleviates the often adopted assumption of perfect sink through the introduction of a kinetic parameter in the phase-field equations related to the dislocation jog density.

iv. Since it is based on a phase-field approach, this model can easily take into account a high diversity of microstructural defects interacting with each other, allowing to investigate multi-sink effects, which remains quite scarce in the literature. For example, this is done in this paper to investigate the effect of the presence of a grain boundary (mimicked by a planar sink) on the dislocation climb rate in pure bcc iron.

v. The model includes a multi-time step algorithm in order to couple phenomena with different characteristic time scales by several orders of magnitude, namely climb, PD and chemical diffusion, since all these phenomena interact with each other under irradiation.

Thanks to these new methodological tools, we obtain the following salient results:

vi. A preliminary generic study of dislocations considered as nonperfect sinks leads to nonintuitive results, since the climb rate decreases when the dislocation jog density increases.

vii. After the model validation, the growth of a <100>-type interstitial loop mimicked by a dipole of edge dislocations was simulated in pure bcc iron in the presence of another neutral sink. The results show that the thermal equilibrium fractions of PD play a significant role on the climb rate calculations, especially at high temperatures. Moreover, the climb rate increases with the simultaneous increase of the temperature and decrease of the dislocation density.

viii. The RIS phenomenon was simulated near the same type of loop during its growth in Fe-%11Cr alloy at 700 K. For a realistic climb rate the size and shape of the Cr atmosphere, and the Cr segregation level and tendency around the dislocation cores are modified. Thus, the sink mobility can play an important role on the RIS prediction.

All these results illustrate the relevance of the proposed dislocation climb PF model to investigate a new panel of phenomena involving dislocations under irradiation (irradiation creep, irradiation void swelling, multi-sink effects, ...).

Declaration of Competing Interest

None.

Credit author statement

Gabriel F. Bouobda Moladje: Conceptualization, Methodology, Software, Validation, Formal Analysis, Investigation, Writing - Original draft. **Ludovic Thuinet**: Conceptualization, Methodology, Resources, Writing - Original draft, Supervision, Project Administration. **Charlotte S. Becquart**: Resources, Writing - Original draft, Supervision, Project Administration, Funding Acquisition. **Alexandre Legris**: Resources, Writing - Original draft, Supervision, Project Administration, Funding Acquisition.

Acknowledgements

- This work was supported by the Euratom research and training programme 2015-2019 under Grant Agreement No 661913 (SOTERIA).
- The authors thank the Centre de Ressources Informatiques of the université de Lille (CRI) for computational facilities.

Data Availability

The raw/processed data required to reproduce these findings cannot be shared at this time as the data also forms part of an ongoing study.

References

[1] D. Caillard, J. L. Martin, Thermally Activated Mechanisms in Crystal Plasticity, Pergamon, Amsterdam, 2003.

[2] R. A. Lebensohn, C. S. Hartley, C. N. Tomé, O. Castelnau, Modeling the mechanical response of polycrystals deforming by climb and glide, Philosophical Magazine 90 (2010) 567–583. doi:10.1080/14786430903213320.

[3] F. D. Fischer, J. Svoboda, Chemically and mechanically driven creep due to generation and annihilation of vacancies with non-ideal sources and sinks, International Journal of Plasticity 27 (2011) 1384–1390. doi:10.1016/j.ijplas.2011.03.005.

[4] M. Basirat, T. Shrestha, G. P. Potirniche, I. Charit, K. Rink, A study of the creep behavior of modified 9Cr-1Mo steel using continuum-damage modeling, International Journal of Plasticity 37 (2012) 95–107. doi:10.1016/j.ijplas.2012.04.004.

[5] B. Babu, L.-E. Lindgren, Dislocation density based model for plastic deformation and globularization of Ti-6Al-4V, International Journal of Plasticity 50 (2013) 94–108. doi:10.1016/j.ijplas.2013.04.003.

[6] M. G. D. Geers, M. Cottura, B. Appolaire, E. P. Busso, S. Forest, A. Villani, Coupled glide-climb diffusion-enhanced crystal plasticity, Journal of the Mechanics and Physics of Solids 70 (2014) 136–153. doi:10.1016/j.jmps.2014.05.007.

[7] S. V. Bobylev, A. K. Mukherjee, I. A. Ovid'ko, A. G. Sheinerman, Effects of intergrain sliding on crack growth in nanocrystalline materials, International Journal of Plasticity 26 (2010) 1629–1644. doi:10.1016/j.ijplas.2010.03.001.

[8] J. Wang, I. J. Beyerlein, C. N. Tomé, Reactions of lattice dislocations with grain boundaries in Mg: Implications on the micro scale from atomic-scale calculations, International Journal of Plasticity 56 (2014) 156 – 172. doi:https://doi.org/10.1016/j.ijplas.2013.11.009.

[9] H. Xie, K. Xu, G.-H. Lu, T. Yu, F. Yin, Dislocation climbing mechanism for helium bubble growth in tungsten, Scripta Materialia 147 (2018) 98–102. doi:10.1016/j.scriptamat.2018.01.009.

[10] D. Mordehai, E. Clouet, M. Fivel, M. Verdier, Introducing dislocation climb by bulk diffusion in discrete dislocation dynamics, Philosophical Magazine 88 (2008) 899 – 925. doi:10.1080/14786430801992850.

[11] Y. Gao, Z. Zhuang, Z. L. Liu, X. C. You, X. C. Zhao, Z. H. Zhang, Investigations of pipe-diffusion-based dislocation climb by discrete dislocation dynamics, International Journal of Plasticity 27 (2011) 1055 – 1071. doi:https://doi.org/10.1016/j.ijplas.2010.11.003.

[12] K. M. Davoudi, L. Nicola, J. J. Vlassak, Dislocation climb in two-dimensional discrete dislocation dynamics, Journal of Applied Physics 111 (2012) 103522. doi:10.1063/1.4718432.

[13] S. M. Keralavarma, T. Cagin, A. Arsenlis, A. A. Benzerga, Power-law creep from discrete dislocation dynamics, Physical Review Letters 109 (2012) 265504. doi:10.1103/physrevlett.109.265504.

[14] C. Ayas, J. A. W. van Dommelen, V. S. Deshpande, Climb-enabled discrete dislocation plasticity, Journal of the Mechanics and Physics of Solids 62 (2014) 113–136. doi:10.1016/j.jmps.2013.09.019.

[15] M. Huang, Z. Li, J. Tong, The influence of dislocation climb on the mechanical behavior of polycrystals and grain size effect at elevated temperature, International Journal of Plasticity 61 (2014) 112 – 127. doi:https://doi.org/10.1016/j.ijplas.2014.06.002.

[16] X. Niu, T. Luo, J. Lu, Y. Xiang, Dislocation climb models from atomistic scheme to dislocation dynamics, Journal of the Mechanics and Physics of Solids 99 (2017) 242 – 258. doi:https://doi.org/10.1016/j.jmps.2016.11.012.

[17] Y. U. Wang, Y. M. Jin, A. M. Cuitiño, A. G. Khachaturyan,

Nanoscale phase field microelasticity theory of dislocations: model and 3D simulations, Acta Materialia 49 (2001) 1847–1857. doi:10.1016/s1359-6454(01)00075-1.

[18] M.-A. Louchez, L. Thuinet, R. Besson, A. Legris, Microscopic phase-field modeling of hcp|fcc interfaces, Computational Materials Science 132 (2017) 62–73. doi:10.1016/j.commatsci.2017.02.012.

[19] D. Rodney, Y. L. Bouar, A. Finel, Phase field methods and dislocations, Acta Materialia 51 (2003) 17–30. doi:10.1016/s1359-6454(01)00379-2.

[20] V. I. Levitas, D. W. Lee, D. L. Preston, Interface propagation and microstructure evolution in phase field models of stress-induced martensitic phase transformations, International Journal of Plasticity 26 (2010) 395 – 422. doi:https://doi.org/10.1016/j.ijplas.2009.08.003.

[21] Y. Wang, J. Li, Phase field modeling of defects and deformation, Acta Materialia 58 (2010) 1212–1235. doi:10.1016/j.actamat.2009.10.041.

[22] I. J. Beyerlein, A. Hunter, Understanding dislocation mechanics at the mesoscale using phase field dislocation dynamics, Philosophical Transactions of the Royal Society A 374 (2016) 20150166. doi:10.1098/rsta.2015.0166.

[23] Y. Zeng, A. Hunter, I. J. Beyerlein, M. Koslowski, A phase field dislocation dynamics model for a bicrystal interface system: An investigation into dislocation slip transmission across cube-on-cube interfaces, International Journal of Plasticity 79 (2016) 293 – 313. doi:https://doi.org/10.1016/j.ijplas.2015.09.001.

[24] S. Zheng, Y. Ni, L. He, Phase field modeling of a glide dislocation transmission across a coherent sliding interface, Modelling and Simulation in Mate-

rials Science and Engineering 23 (2015) 035002. doi:10.1088/0965-0393/23/3/035002.

[25] S. Zheng, D. Zheng, Y. Ni, L. He, Improved phase field model of dislocation intersections, njp Computational Materials 4 (2018) 20. doi:10.1038/s41524-018-0075-x.

[26] L. Wang, Z. Liu, Z. Zhuang, Developing micro-scale crystal plasticity model based on phase field theory for modeling dislocations in heteroepitaxial structures, International Journal of Plasticity 81 (2016) 267 – 283. doi:https://doi.org/10.1016/j.ijplas.2016.01.010.

[27] J. Ke, A. Boyne, Y. Wang, C. Kao, Phase field microelasticity model of dislocation climb: Methodology and applications, Acta Materialia 79 (2014) 396–410. doi:10.1016/j.actamat.2014.07.003.

[28] P.-A. Geslin, B. Appolaire, A. Finel, A phase field model for dislocation climb, Applied Physics Letters 104 (2014) 011903. doi:10.1063/1.4860999.

[29] P.-A. Geslin, B. Appolaire, A. Finel, Multiscale theory of dislocation climb, Physical Review Letters 115 (2015) 265501. doi:10.1103/physrevlett.115.265501.

[30] P. Liu, S. Zheng, K. Chen, X. Wang, B. Yan, P. Zhang, S. Q. Shi, Point defect sink strength of low-angle tilt grain boundaries: A phase field dislocation climb model, International Journal of Plasticity 119 (2019) 188 – 199. doi:https://doi.org/10.1016/j.ijplas.2019.03.008.

[31] Y. Li, S. Hu, X. Sun, M. Stan, A review: applications of the phase field method in predicting microstructure and property evolution of irradiated

nuclear materials, npj Computational Materials 3 (2017) 16. doi:10.1038/s41524-017-0018-y.

[32] P. Bellon, Phase field methods, Comprehensive Nuclear Materials 1 (2012) 411–432. doi:10.1016/b978-0-08-056033-5.00031-8.

[33] Y. Li, S. Hu, C. H. H. Jr, H. Deng, F. Gao, X. Sun, M. A. Khaleel, Computer simulations of interstitial loop growth kinetics in irradiated bcc Fe, Journal of Nuclear Materials 427 (2012) 259–267. doi:10.1016/j.jnucmat.2012.05.004.

[34] H. Rouchette, L. Thuinet, A. Legris, A. Ambard, C. Domain, Quantitative phase field model for dislocation sink strength calculations, Computational Materials Science 88 (2014) 50–60. doi:10.1016/j.commatsci.2014.02.011.

[35] L. Thuinet, H. Rouchette, A. Legris, 3D phase-field modelling of dislocation loop sink strengths, Journal of Nuclear Materials 483 (2017) 62–81. doi:10.1016/j.jnucmat.2016.10.041.

[36] A. H. Duparc, C. Moingeon, N. S. de Grande, A. Barbu, Microstructure modelling of ferritic alloys under high flux 1 MeV electron irradiations, Journal of Nuclear Materials 302 (2002) 143–155. doi:10.1016/s0022-3115(02)00776-6.

[37] R. B. Adamson, C. E. Coleman, M. Griffiths, Irradiation creep and growth of zirconium alloys: A critical review, Journal of Nuclear Materials 521 (2019) 167–244. doi:10.1016/j.jnucmat.2019.04.021.

[38] M. Nastar, F. Soisson, Radiation-induced segregation, Comprehensive Nuclear Materials 1 (2012) 471–496. doi:10.1016/b978-0-08-056033-5.00035-5.

[39] J. B. Piochaud, M. Nastar, F. Soisson, L. Thuinet, A. Legris, Atomic-based phase-field method for the modeling of radiation induced segregation in Fe–Cr, Computational Materials Science 122 (2016) 249–262. doi:10.1016/j.commatsci.2016.05.021.

[40] L. Thuinet, M. Nastar, E. Martinez, G. B. Moladje, A. Legris, F. Soisson, Multiscale modeling of radiation induced segregation in iron based alloys, Computational Materials Science 149 (2018) 324–335. doi:10.1016/j.commatsci.2018.03.024.

[41] G. S. Was, Fundamentals of radiation materials science: metals and alloys, Springer (2007) .doi:10.1016/s1369-7021(07)70250-x.

[42] A. Khachaturyan, Theory of structural transformations in solids, Wiley (1983) .

[43] F. R. N. Nabarro, The synthesis of elastic dislocation fields, Philosophical Magazine 42 (1951) 1224–1231. doi:10.1080/14786444108561379.

[44] S. Y. Hu, J. Choi, Y. L. Li, L. Q. Chen, Dynamic drag of solute atmosphere on moving edge dislocations - phase-field simulation, Journal of Applied Physics 96 (2004) 229. doi:10.1063/1.1755858.

[45] S. Hu, Y. Lia, Y. Zheng, L. Chen, Effect of solutes on dislocation motion - a phase-field simulation, International Journal of Plasticity 20 (2004) 403–425. doi:10.1016/s0749-6419(03)00094-9.

[46] L. Thuinet, A. D. Backer, A. Legris, Phase-field modeling of precipitate evolution dynamics in elastically inhomogeneous low-symmetry systems: Application to hydride precipitation in Zr, Acta Materialia 60 (2012) 5311–5321. doi:10.1016/j.actamat.2012.05.041.

[47] Thuinet, A. Legris, L. Zhang, A. Ambard, Mesoscale modeling of coherent zirconium hydride precipitation under an applied stress, Journal of Nuclear Materials 438 (2013) 32–40. doi:10.1016/j.jnucmat.2013.02.034.

[48] G. Oum, L. Thuinet, A. Legris, A 3D crystal plasticity model for coherency loss during precipitation, Modelling and Simulation in Materials Science and Engineering 26 (2018) 065008. doi:10.1088/1361-651x/aacfdb.

[49] L. Onsager, Reciprocal relations in irreversible processes. i., Physical Review 37 (1931) 405–426. doi:10.1103/physrev.37.405.

[50] L. Onsager, Reciprocal relations in irreversible processes. ii., Physical Review 38 (1931) 2265–2279. doi:10.1103/physrev.38.2265.

[51] P.-A. Geslin, Contribution à la modélisation champ de phase des dislocations, Ph.D. thesis (2013).

[52] H. Rauh, D. Simon, On the diffusion process of point defects in the stress field of edge dislocations, physica status solidi (a) 42 (1978) 499–510. doi:10.1002/pssa.2210460213.

[53] E. A. Little, Neutron-irradiation hardening in irons and ferritic steels, International Metals Reviews 21 (1976) 25–60. doi:10.1179/imtr.1976.21.1.25.

[54] I. M. Robertson, M. Jenkins, C. English, Low-dose neutron-irradiation damage in alpha-iron, Journal of Nuclear Materials 108-109 (1982) 209–221.

[55] L. L. Horton, J. Bentley, K. Farrell, A TEM study of neutron-irradiated iron, Journal of Nuclear Materials 108-109 (1982) 222–233. doi:10.2172/6659613.

[56] M. Mendelev, S. Han, D. Srolovitz, G. Ackland, D. sun, M. Asta, Development of new interatomic potentials appropriate for crystalline and liquid iron, Philosophical Magazine 83 (2003) 3977–3994. doi:10.1080/14786430310001613264.

[57] L. Malerba, M. Marinica, N. Anento, C. Björkas, H. Nguyen, C. Domain, F. Djurabekova, P. Olsson, K. Nordlund, A. Serra, D. Terentyev, F. Willaime, C. Becquart, Comparison of empirical interatomic potentials for iron applied to radiation damage studies, Journal of Nuclear Materials 406 (2010) 19–38. doi:10.1016/j.jnucmat.2010.05.017.

[58] P. Yvon, F. Carré, Structural materials challenges for advanced reactor systems, Journal of Nuclear Materials 385 (2) (2009) 217–222. doi:10.1016/j.jnucmat.2008.11.026.

[59] P. Ehrhart, K. Robrock, H. Schober, Physics of radiation effects in crystals, Elsevier, Amsterdam (1986) 63.

[60] V. I. Levitas, M. Javanbakht, Thermodynamically consistent phase field approach to dislocation evolution at small and large strains, Journal of the Mechanics and Physics of Solids 82 (2015) 345–366. doi:10.1016/j.jmps.2015.05.009.